Journal of Sound and Vibration (2000) **237**(2), 281–302
doi:10.1006/jsvi.2000.3057, available online at http://www.idealibrary.com on IDEAL®

POWER VARIANCES AND DECAY CURVATURE IN A REVERBERANT SYSTEM

Oleg I. Lobkis, Richard L. Weaver and Igor Rozhkov

Theoretical & Applied Mechanics, University of Illinois, Urbana, IL 61801, *U.S.A.*

(*Received* 18 *November* 1999, *and in final form* 29 *March* 2000)

Laboratory measurements of the variance of the power transmission coefficient for ultrasound in a reverberant elastic body are compared with extant theory and found to agree. The theory is then extended to describe the transition between behaviors at low and high modal overlap and to incorporate the effects of decay curvature. The new and more precise theory is found to agree poorly with measurements. Reasons for the poor agreement are discussed; it is concluded that the only viable hypothesis is that mode shape statistics are not described by real Gaussian random functions.

1. INTRODUCTION

In a series of papers some years ago Davy [1–3] presented an extensive study of power variances in reverberation rooms, the chief aim of which was to provide a better understanding of errors in power estimates for narrow band noise sources. His work confirmed and modified and extended earlier studies [4, 5] in which it was concluded that the variance in a reverberation room measurement of steady state power depends strongly on the modal overlap $M = 2\pi\gamma D$, where D is the modal density (modes per unit frequency $d\omega$) and γ is the dissipation rate (units of nepers per time) of acoustic amplitude. At larger overlap the relative variance is unity, i.e., the expected fluctuations in the measured power are comparable to the power itself. This is precisely what one would conclude from a model in which the transient room response was a Gaussian random process under an exponential decay envelope.

At weak overlap the variance is much larger. Early theory [4] based on an assumption of uncorrelated eigenfrequencies suggested it should be $1 + K^2/M$ for all M, with K related to the statistics of the mode shapes, equal to $\langle u^4\rangle/\langle u^2\rangle^2$, the ratio of the mean fourth power of a mode amplitude to the square of the mean square. K was commonly taken to be 27/8, as if the modes had the statistics of the oblique modes in a three-dimensional rectangular room.

A variance larger than unity at small M is easily understood if one recalls that, at small M, the modes are relatively distinct. In this case the room response varies strongly as the frequency of excitation coincides, or not, with an eigenfrequency of the room.

Davy [1–3] and Lyon [4] showed that this formula is modified if the eigenfrequencies are not independent random numbers. They discussed the effects of an assumption called nearest-neighbor level repulsion and obtained $1 + (K^2 - 3/2)/M$ at large M. Weaver [6], however, pointed out that the nearest-neighbour assumption of Lyon and Davy lacks the long-range correlations predicted by random matrix theory [7–9]. Retaining the standard assumption that all modes in a given frequency range have identical modal decay rates γ, Weaver [6] then showed that the eigenfrequency correlations derived from the Gaussian

0022-460X/00/420281 + 22 $35.00/0

orthogonal ensemble of random matrix theory modifies the formula further. Like other Weaver obtained $1 + K^2/M$ at small M. But at large M he showed that long-range sepctral rigidity leads to the expression $1 + (K^2 - 3)/M$ at large modal overlap.

The theory of random matrices predicts the "Gaussian orthogonal ensemble" [8, 9] form for the eigenfrequency correlations. But questions remain as to the applicability of that theory. The GOE correlations have been confirmed in measurements in reverberation rooms [10], in microwave cavities [11] and in elastic bodies [7, 12, 13]. It is widely believed that the theory of random matrices applies to such systems if their ray trajectories are chaotic [14, 15]. However, it has been shown [16–19] that chaos *per se* is not necessary in order for the GOE eigenfrequency correlations to be obeyed to good accuracy and great range. One needs only breaking of symmetries and a certain amount of diffuse scattering.

Random matrix theory further predicts that the eigenmodes are Gaussian random processes in space. This implies that K should equal 3, a result that also follows if the modes are written, locally, as random superpositions of real plane waves. The value $K = 3$ has been supported by numerous numerical experiments on systems with chaotic ray trajectories [20, 21] and systems with large amounts of diffuse scattering [22], and is predicted by the theory of random matrices [8, 9, 23]. The conclusion has been that the relative variance should be $1 + 9/M$ at low M and $1 + 6/M$ at large M. A prediction for the regime between these to limits has not yet been made, though it is reasonable to suppose that the transition is smooth and monotonic.

Understanding power variances in reverberant systems not only has implications for the accuracy of power measurements in reverberation rooms, but it also has a potential application to the measurement of modal density. If decay γ can be measured independently, and if the relative variance can also be measured, modal density follows from an expression relating relatively variance to M. Thus, modal density could be measurable even if the modes have strong overlap.

This is the chief motivation for the present work. It has been suggested that the modal density is a natural way to ultrasonically characterize heterogeneous media at wavelengths for which one cannot propagate a coherent wave and so cannot measure wave speed. In the search for Anderson localization of classical waves, the modal density is a key parameter [24]. Modal density is also a key parameter for statistical energy analysis [25].

In the next section, we present an experimental study of a small aluminum block, its diffuse energy decay rate, σ, and its power variance. With the known modal density, given by the standard short-wavelength asymptotic formula, we then compare the observed variance with the theory discussed above.

In making this comparison we find two significant difficulties. Inasmuch as the decay is not purely exponential, it is not clear how the decay should be characterized, and in particular, what value should be assigned to γ. After resolving this issue by fitting the decay to a model with curvature, we extract a value for the mean amplitude decay rate $\langle\gamma\rangle$. The theoretical and measured variances are then compared and found to be in reasonable correspondence, thus motivating a closer scrutiny of the uncertainties in the above theory for the variance.

For this reason, the subsequent section presents a more complete theory of power variance than heretofore exists in the literature. Here we calculate the full M dependence of the relative variance, including the transition between $1 + 9/M$ and $1 + 6/M$. We also extend the theory to the case in which the modes are assumed to have different decay rates, drawn from a narrow distribution consistent with the model we used for fitting the decay curvature.

The agreement between measured and theoretical variance is found to be worsened. An extensive discussion of the possible reasons for poor agreement with theory then follows

and it is reluctantly concluded that the only viable conjecture is that $K < 3$. This is, the modes of the sample studied are not real Gaussian random functions of space.

2. MODAL DENSITY, DECAY, AND POWER VARIANCE IN A SAMPLE SYSTEM

2.1. DESCRIPTION OF MEASUREMENT PROCEDURE

We study, as a representative reverberant system, a small aluminum block with nominal dimensions of $25 \times 25 \times 37$ mm; it is the same block that was called "block A" in an earlier report [7]. It is illustrated in Figure 1. A single oblique slit made by a band saw serves to break the three reflection symmetries of the original rectangular block. The slit, of width 1 mm, also provides a source of diffuse scattering; elastic waves will diffract from its tip and its base. Two thin Valpey–Fisher pin transducers are used as transient wide-band ultrasonic sources and receivers (diameter 1·5 mm each, element diameter 1·0 mm). In order to minimize absorption, they are applied to the surface without liquid couplant. The source transducer is excited by a high-voltage pulse for a duration of a few nanoseconds.

The received signal is amplified by 40 dB and captured by a 32 000 word 8-bit waveform digitizer at a sampling rate of 5 MS/s. The captured waveform is then repetition averaged, typically 50 times, to improve signal-to-noise ratios. The resulting transient decaying signals had useful durations between 50 and 70 ms and useful components up to about 1·9 MHz (where the shear wave length $\lambda_{shear} \approx 1{\cdot}6$ mm). This wave capture was repeated with various trigger delays in order to access the full record, a record with a length of the order of 300 000 words. Repetition averaging and variable voltage scales resulted in a dynamic range considerably greater than 8 bits.

A typical waveform is shown in Figure 1. It appears to be wide-band noise under a decaying envelope. A more precise description requires time–frequency analysis. As has been described elsewhere [26] the signal is therefore time-windowed by Δt (with cosine-bell edges), Fourier-transformed, squared, and finally integrated over short ranges Δf in

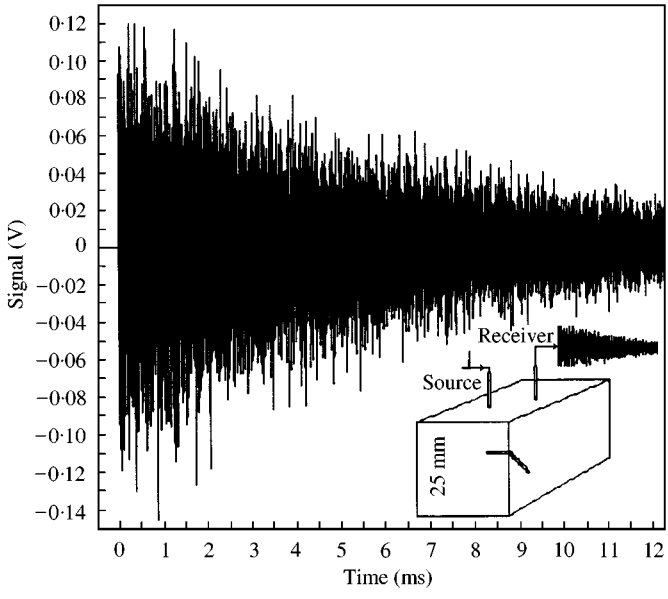

Figure 1. The first several ms of a typical waveform. The signal has the appearance of noise under a decaying envelope. Block 'A' is illustrated in the inset.

frequency. Typically, $\Delta t = 205$–$820\ \mu s$ and $\Delta f = 39$ or 78 kHz. The result is the spectral energy density $E(t, f)$ for a set of time windows and frequency bins. A plot of the logarithm of $E(t, f)$ versus time is shown, for several different frequencies, in Figure 2. At each frequency the energy decays in a manner that is approximately exponential. The rate of that decay, $\sigma = -\,\mathrm{d}\ln E/\mathrm{d}t$, is a measure of the dissipation in the structure.

It is clear from Figure 2 that a straight-line fit would be nearly adequate in one case (at high frequency) but would fail, to a statistically significant degree, in other cases. The lower frequencies manifest a decay curvature. Inasmuch as knowing the decay rate is critical for the present program, it is necessary to come to some understanding of the source of this curvature, and in particular what value to use for γ. At high frequencies it seems evident that $\gamma = \sigma/2$ is appropriate. At low frequencies the slope $-\,\mathrm{d}\ln E/\mathrm{d}t$ is not constant, so the identification $\gamma = \sigma/2$ is ambiguous.

One could hypothesize that the curvature is an artefact of the signal processing. If σ depends on frequency (and it does) and if the frequency bins are sufficiently wide, then the energy in one frequency bin contains components with different frequencies and hence different decay rates. One consequence would be decay curvature with a sense like that in Figure 2. The amount of curvature would, though, depend on the frequency bin widths Δf. We have found that changing Δf does not (except as noted below) change the curvature. We are left with a need to find a deeper cause for the curvature. This is an issue that has been addressed in the recent literature.

2.2. FITS TO CURVED DECAY PROFILES

In a recent series of papers by Burkhardt and co-workers [27, 28], it has been suggested that the decay curvature is a product of variation amongst modal decay rates, even between modes at almost the same frequency. Inasmuch as a simple perturbative estimate for the modal decay rate suggests that the decay rate should depend on the details in the shape of the associated eigenmode, one expects random fluctuations in these modal decay rates. Based on a simple model in which dissipation is confined to a modest number, $2n$, of isolated equipotent points in the body, and in which the mode shapes are Gaussian random processes in space, Burkhardt *et al.* show that the modal decay rates should be distributed in accordance with a chi-square distribution of the same order,

$$p(\gamma)\,\mathrm{d}\gamma \propto \gamma^{n-1} \exp(-n\gamma/\bar{\gamma})\,\mathrm{d}\gamma, \tag{1}$$

where $\bar{\gamma} = \sigma/2$ is the average γ.

Such a distribution of modal decay rates leads to an estimate for diffuse energy given by an incoherent superposition of modes of different γ's. Each mode has an energy decaying like $\sim \exp(-2\gamma t)$, so the superposition has an energy decay given by $p(\gamma)$'s Laplace transform

$$E(t) \sim \int_0^\infty p(\gamma) \exp(-2\gamma t)\,\mathrm{d}\gamma, \qquad E(t) = E_0(1 + \sigma t/n)^{-n}. \tag{2}$$

As $n \Rightarrow \infty$ one recovers conventional exponential decay $\sim \exp(-\sigma t)$. One may also note that, for early times t, $\ln E \sim -\sigma t + (\sigma t)^2 + 2n - (\sigma t)^3/3n^2 + \cdots$, i.e., the decay commences at the average rate. Burkhardt has suggested [28] that the parameter n, inasmuch as it is related to the number of a distinct sites at which dissipation is significant, might correlate with the presence of localized damage.

In any case, the model gives a plausible form for the curvature. Fits of $E(t)$ to form (2) yield estimates for the average modal width, $\bar{\gamma} = \sigma/2$, and for the curvature parameter n.

Some of the fits to equation (2) are shown in Figure 2; the recovered values for σ and n are shown in Figure 3.

The quality of the fit to the three-parameter form is remarkable, especially in view of the simplicity of the model from which it was derived. Chi-squares of the fit were found to be

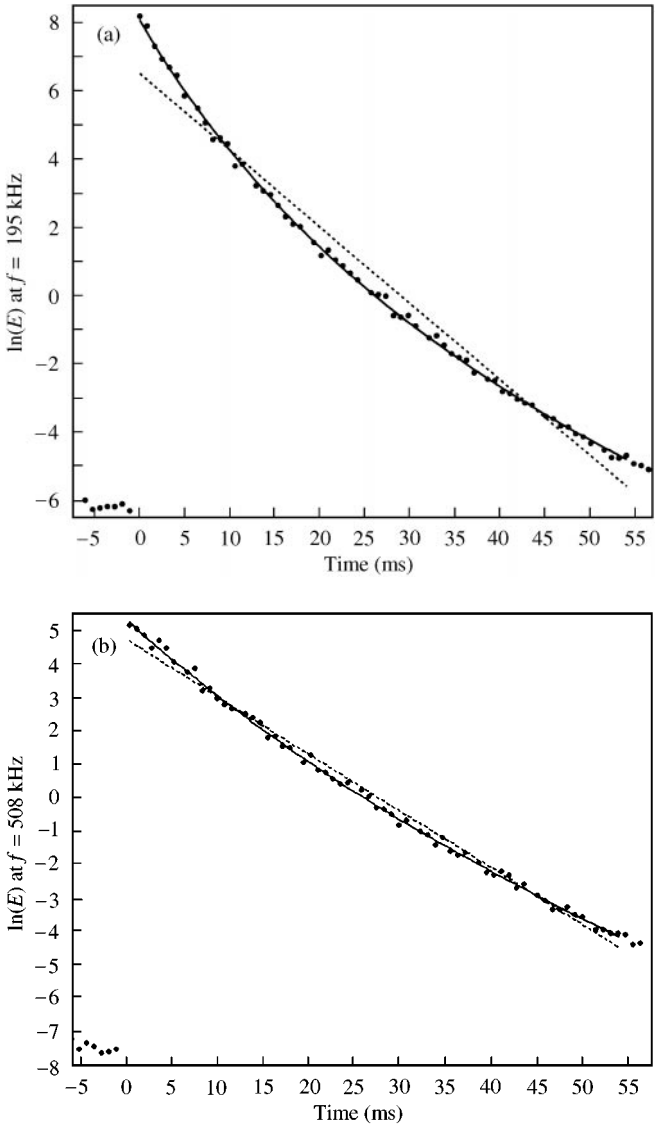

Figure 2. (a) The logarithm of the observed spectral energy density at 195 kHz is plotted versus time. The residual noise level is apparent from the data at negative times. The signal stays well above the noise for 60 ms. The decay is fit to two different theories. The conventional linear decay (- - - -) is obviously contradicted by the data. The three-parameter fit to a curved decay (——) fits the data quite well. Fit parameters are as follows. Linear fit: $E_0 = 6{\cdot}578$, $\sigma = 0{\cdot}227$, chi-square $= 23{\cdot}97$; curved fit: $E_0 = 8{\cdot}244$, $\sigma = 0{\cdot}4705$, $n = 10{\cdot}96$, chi-square $= 0{\cdot}813$. (b) The logarithm of the observed spectral energy density at 508 kHz is plotted versus time. The conventional linear decay is obviously contradicted by the data. The three-parameter fit to a curved decay fits the data quite well. Fit parameters are as follows. Linear fit $E_0 = 4{\cdot}755$, $\sigma = 0{\cdot}1713$, chi-square $= 2{\cdot}346$; curved fit: $E_0 = 5{\cdot}34$, $\sigma = 0{\cdot}2435$, $n = 15{\cdot}38$, chi-square $= 0{\cdot}851$. (c) The logarithm of the observed spectral energy density at 1602 kHz is plotted versus time. The decay is fit to two different theories. The conventional linear decay and the three-parameter curved decay both fit the data, though the curved decay model fits better. Fit parameters are as follows. Linear fit $E_0 = 4{\cdot}586$, $\sigma = 0{\cdot}2094$, chi-square $= 2{\cdot}662$; curved fit: $E_0 = 4{\cdot}948$, $\sigma = 0{\cdot}251$, $n = 34{\cdot}7$, chi-square $= 1{\cdot}047$.

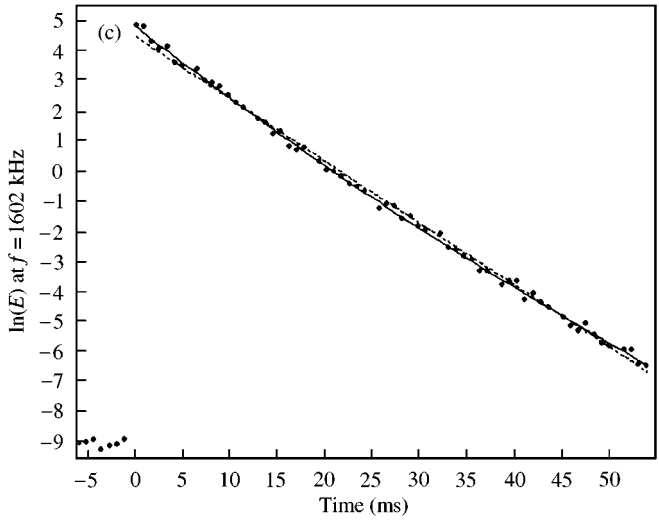

Figure 2. Continued.

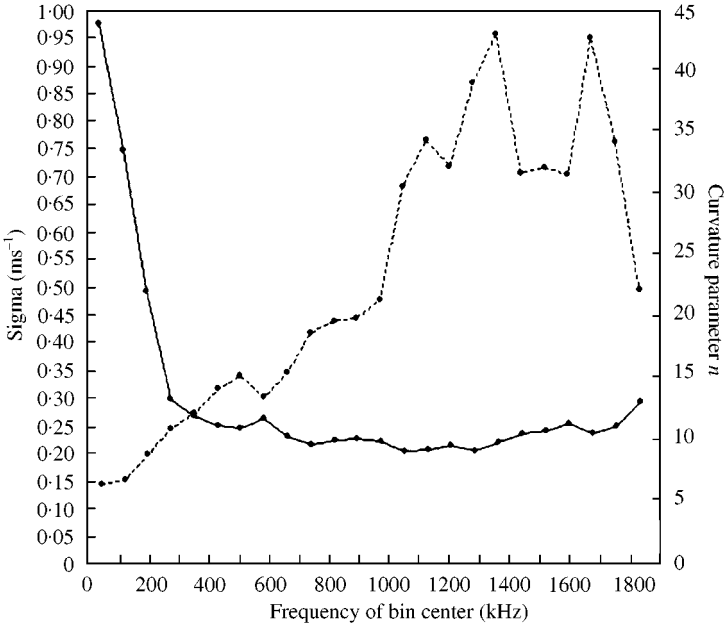

Figure 3. The fit parameters σ (——) and n (- - - -), averaged over fits to several sets of data from different positions of source and receiver, are plotted versus frequency. The unexpected large absorption at very low frequencies is attributed to unknown mechanisms in the specimen's support. At high frequencies where the curvature is slight, n is large.

fully acceptable (that is, the data do not contradict the model), whereas the chi-squares of a fit to the simpler model $E_0 \exp(-\sigma t)$ indicate that the data do contradict that simpler model. One could also hypothesize an alternative form for the curved decay: $E_0 \exp(-\sigma t + \beta t^2)$ (which follows from an assumption of a Gaussian distribution of modal decay rates). We find that an attempt to fit to the alternative form results in poor chi-squares.

One could also entertain the hypothesis that the curvature is not directly related to the dissipation, but rather a consequence of a non-linearity somewhere in the system, either the elastic waves or the transducers or the amplifier or the digitizer. If, for example, the amplifier had more gain at low levels than at high levels, the weaker signals at late times would be enhanced relative to the stronger signals at early times. Curvature like that shown in Figure 2 would be one consequence. We have examined this hypothesis by varying the source pulse amplitude (over a range of 25 dB) and found the shapes of the $\ln E$ versus t plots to be unchanged. We have also (at low frequencies where modal overlap is small enough that it is possible) reduced Δf sufficiently that only one mode lies in a bin; the resulting plot then shows no curvature. Thus, individual modes decay without curvature and the cause of the curvature is not non-linearity.

The picture of curvature as related to variations in modal decay rates is corroborated by a study, at low frequencies where it is possible to distinguish the modes, of the means and standard deviations of the widths of the peaks in the Fourier transform of the entire waveform. The widths have means and variances consistent with the assumed distribution (2) and with the values for σ and n recovered from our fits to the decay of the diffuse signal.

2.3. THEORY FOR MODAL DENSITY

Estimates for M also require estimates for modal density. In bulk elastodynamic bodies the modal density is describable, for asymptotically high frequency, by a Weyl-like series. The leading term of this series is proportional to the volume V of the body and to the square of the frequency. For an isotropic material the term is simply related to the equivoluminal and dilatational wave speeds, c_e and c_d [29]. It is found by standard mode-counting procedures

$$(V/2\pi^2)\,[\omega^2/c_d^3 + 2\omega^2/c_e^3].$$

The next term in the asymptotic series is proportional to the surface area S of the body and was derived for traction-free surfaces by Dupuis *et al.* [30],

$$(S\omega/8\pi c_d^2)\,[2-3(c_d/c_e)^2 + 3(c_d/c_e)^4]/[(c_d/c_e)^2 - 1].$$

There is, presumably, a third term in the series, independent of frequency and proportional to the amount of perimeter L. Our asymptotic estimate for the modal density is then

$$\mathrm{d}N/\mathrm{d}\omega = D(\omega) = (V/2\pi^2)[\omega^2/c_d^3 + 2\omega^2/c_e^3] + (S\omega/8\pi c_d^2)\,[2-3(c_d/c_e)^2 + 3(c_d/c_e)^4]/[(c_d/c_e)^2 - 1] + O(L/c). \quad (3)$$

In the low modal overlap regime where we can unambiguously count the modes it is possible to compare this formula with that count. That comparison was made several years ago [7] and the above formula confirmed as accurate, within a few percent, for frequencies between 100 and 200 kHz.

2.4. POWER VARIANCES

In addition to the above estimates for D and for σ, we require measurements of power variances. Previous theories [1–6], and also the theory to be presented in the next section, consider variances across an ensemble of equivalent samples. Here we construct our variances by examining a range of frequencies. There is a kind of ergodicity assumption

implicit in the comparison. Random matrix theory, however, indicates that modal statistics are, in this sense, ergodic.

Power variances are constructed by Fourier transforming the complete waveform, like the one shown in Figure 1, without any time windowing. The absolute value of this Fourier transform is plotted in Figure 4 over some representative short ranges in frequency. While each shows a mean value (that is persumably dependent on transducer efficiency as well as a host of other things) each also shows a substantial fluctuation away from that mean. We see that the low-frequency case in Figure 4(a) has much greater fluctuations than does the

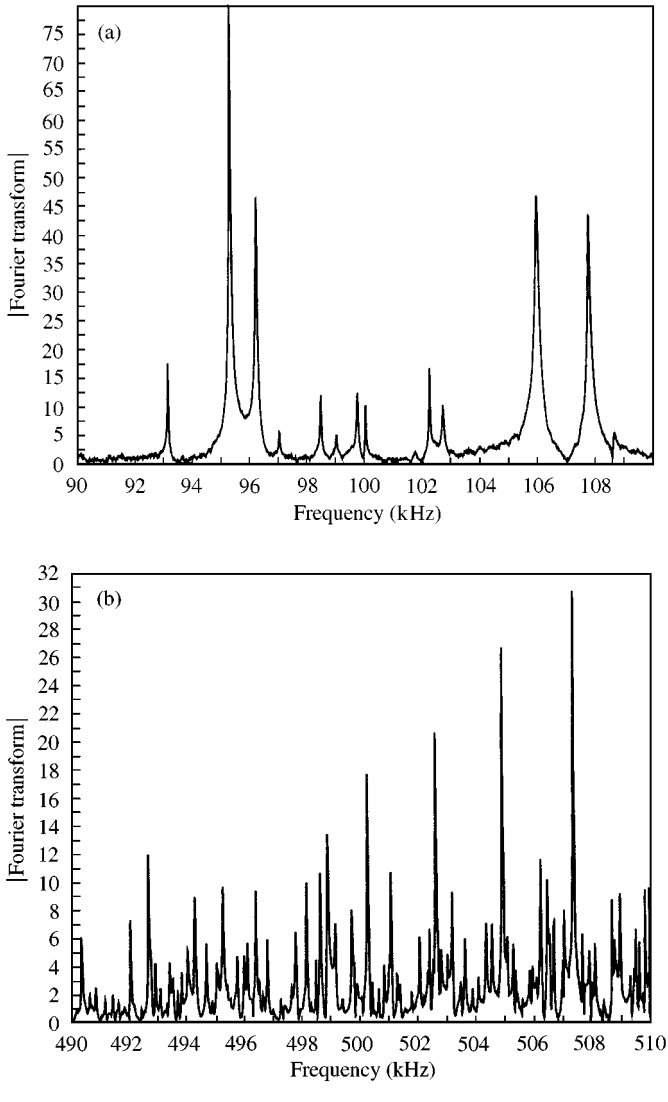

Figure 4. (a) The absolute value of the Fourier transform of the signal, in the range around 100 kHz. We note distinct peaks at the natural frequencies of the specimen and the variance amongst the peak amplitudes. The peaks are well separated, as the modal overlap at 100 kHz is small. One can also note a variance amongst the peak widths. (b) The absolute value of the Fourier transform of the signal, in the range around 500 kHz. We note distinct peaks at the natural frequencies of the specimen and the variance amongst the peak amplitudes. The peaks are not well separated, as the modal overlap at 500 kHz is significant. (c) The absolute value of the Fourier transform of the signal, in the range around 1500 kHz. Distinct peaks at the natural frequencies of the specimen are not discernable, as the modal overlap at 1500 kHz is large.

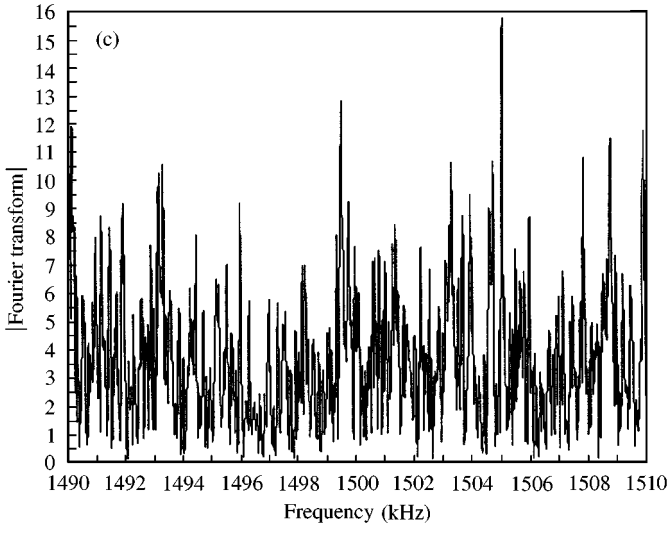

Figure 4. Continued.

intermediate frequency case in Figure 4(b) and the high-frequency case in Figure 4(c). The fluctuation is quantified by the relative variance, defined by

$$relvar = \frac{\langle T^2 \rangle - \langle T \rangle^2}{\langle T \rangle^2} = \frac{(f_2 - f_1)\int_{f_1}^{f_2} T^2(f)\,\mathrm{d}f}{(\int_{f_1}^{f_2} T(f)\,\mathrm{d}f)^2} - 1, \tag{4}$$

where T is the square of the Fourier transform. If the range $\{f_1 \to f_2\}$ is short enough, then the secular variations in the mean, due to the frequency dependence in the tranducer or the system itself, will not contribute to the calculation of *relvar*. If it is too short, then equation (4) will itself fluctuate. If it is much too short, $f_2 - f_1 \ll \gamma/2\pi$, then $\langle T \rangle$ is poorly estimated and *relvar* vanishes.

Relvar, after averaging the value obtained from a set of distinct source and receiver positions, is plotted versus frequency in Figure 5. As expected it drops rapidly with frequency. Superposed on this plot are the theoretical values $1 + K^2/M$ and $1 + (K^2 - 3)/M$ based on $K = 3$ and $M = \pi D\sigma$, where D is taken from equation (3) and σ is taken from the three-parameter fit (2). The agreement is good. The trends are correct and the local fluctuations in the two theoretical *relvars* due to fluctuations in σ are also seen in the measured relvar. The measured *relvar*, as expected, approaches $1 + 9/M$ at low frequency, and $1 + 6/M$ at high frequency.

The quality of the agreement is such that one is driven to ask whether a more exact theory for *relvar* can be obtained. In particular, one wishes a theory for *relvar* that covers the transition regime between $1 + 9/M$ at small M and $1 + 6/M$ at large M. One also wishes a theory that incorporates variations in modal decay rates. This is the subject of the next section.

3. POWER VARIANCES IN THE TRANSITION REGIME

3.1. AN IMPROVED THEORY

The modal representation for the response (in the i direction, at position $\mathbf{x}$) of a lightly damped elastodynamic body to a unit harmonic point force (in the j direction at

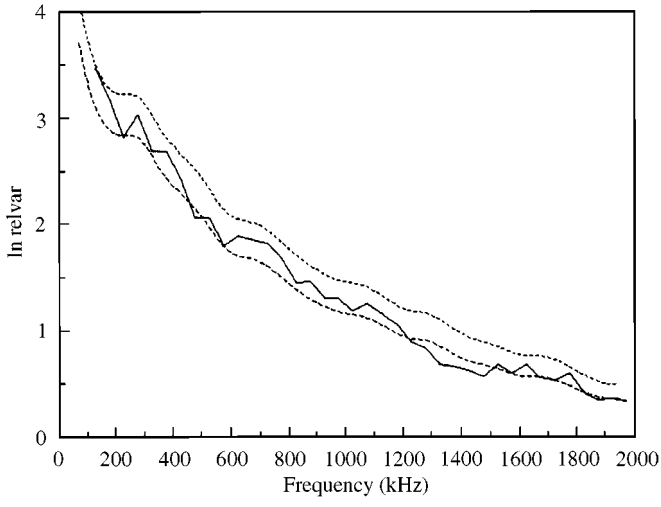

Figure 5. The experimentally determined value for the relative variance is plotted versus frequency (——). The two simple theories $1 + 9/M$ and $1 + 6/M$ are also plotted (- - - -) for comparison. It appears that the actual values lie between the two simple forms, and as expected, approach the latter for large modal overlap.

position **y**) is

$$G_{ij}(\mathbf{x}, \mathbf{y}, \omega) = \sum_r \frac{u_i^r(\mathbf{x})\, u_j^r(\mathbf{y})}{\omega^2 - \omega_r^2 - 2\mathrm{i}\omega\gamma_r}, \tag{5}$$

where $\mathbf{u}^r$ is the rth eigenmode and u_i^r is its ith displacement-vector component. We have presumed, in equation (5), that the system is diagonally damped, i.e., the damping leaves the modes real. This is a common assumption. We do not assume that all modes decay at the same rate γ. We seek G's statistics; in particular we shall calculate the ensemble variance of $|G|^2$, and compare it with the frequency-domain variance found in the experiments.

We shall make several assumptions. As just discussed, the modes are assumed real. We also assume that the eigenfrequencies are not independent random numbers, but rather they have the correlations of the GOE [7–9]. We further assume that the modal decay rates γ_n are independently drawn from the narrow distribution (1), with a mean decay rate $\sigma/2$ and variance related to the curvature parameter n.

As Davy† did [31], we find that equation (5) simplifies if we replace $\omega + \omega_r$ with 2ω,

$$G_{ij}(\mathbf{x}, \mathbf{y}, \omega) \approx \frac{1}{2\omega} \sum_r \frac{u_i^r(\mathbf{x})\, u_j^r(\mathbf{y})}{\omega - \omega_r - \mathrm{i}\gamma_r}. \tag{6}$$

We drop the unimportant prefactor $1/2\omega$ as irrelevant to the calculations of relative variance. The power transmission function T is the absolute-value square of the response

† Davy notes that equation (6) has problematic absolute convergence, and shares this feature with many of the other summations; the problem is not eliminated by avoiding the approximation in equation (6). The difficulty is due to the large number of modes at high index 'r', the density of modes increasing (in three dimensions) quadratically with ω_r. It is our opinion that the matter can be repaired: the summations can be rendered absolutely convergent by replacing the modal factors $u^r(\mathbf{x})$ with the appropriate overlap integral between the eigenmode and a smoothly distribute source or receiver function, e.g. $v^r = \int u^r(\mathbf{x}) S(\mathbf{x})\, \mathrm{d}^3\mathbf{x}$, a quantity which tends rapidly to zero as r goes to infinity. Interestingly, random matrix theory predicts that v^r is Gaussian; K remains three.

$$T = \sum_{r,m} \frac{u_i^r(\mathbf{x})\, u_j^r(\mathbf{y})}{\omega - \omega_r - \mathrm{i}\gamma_r} \frac{u_i^m(\mathbf{x})\, u_j^m(\mathbf{y})}{\omega - \omega_m - \mathrm{i}\gamma_m}. \tag{7}$$

We now take the average across the ensemble, and recognize that different mode shapes are uncorrelated with each other, thus eliminating the $r \neq m$ terms. If $\mathbf{x}$ and $\mathbf{y}$ are far apart, such that the modal amplitudes at those two points are uncorrelated,

$$\langle T \rangle = \sum_r \frac{\langle [u_i^r(\mathbf{x})]^2 [u_j^r(\mathbf{y})]^2 \rangle \equiv \langle u^2 \rangle^2}{(\omega - \omega_r - \mathrm{i}\gamma_r)(\omega - \omega_r + \mathrm{i}\gamma_r)}, \tag{8}$$

where $\langle u^2 \rangle$ is the ensemble average value of the square of an eigenfunction.

We make a further average over the eigenfrequencies by replacing the summation with a factor D and an integral with respect to ω_r,

$$\langle T \rangle = D \langle u^2 \rangle^2 \int_{-\infty}^{\infty} \frac{\mathrm{d}\omega_r}{(\omega - \omega_r - \mathrm{i}\gamma_r)(\omega - \omega_r + \mathrm{i}\gamma_r)}$$

$$= D \langle u^2 \rangle^2 \frac{\pi}{\gamma_r}. \tag{9}$$

The integrand has been approximated with the form it has near the dominating resonance at $\omega_r = \omega$. Thus D denotes the modal density at the frequency ω, thus also the justification for the earlier approximation $\omega + \omega_r \sim 2\omega$. We have examined the more complicated equations that result if these approximations had not been made; we find that the error incurred is small, of order $(\gamma/\omega)^2$.

For a final average we must average over the range (equation (1)) of values of γ

$$\langle T \rangle = D \langle u^2 \rangle^2 \left\langle \frac{\pi}{\gamma} \right\rangle = D \langle u^2 \rangle^2 \frac{\pi}{\bar{\gamma}} \frac{n}{n-1}. \tag{10}$$

where n is the decay curvature parameter defined in equation (2).

The ensemble variance of T is given in terms of $\langle T^2 \rangle$. Again dropping the irrelevant prefactor $1/2\omega$, we find

$$T^2 = \sum_{r,m,l,k} \frac{u_i^r(\mathbf{x})\, u_j^r(\mathbf{y})}{\omega - \omega_r - \mathrm{i}\gamma_r} \frac{u_i^m(\mathbf{x})\, u_j^m(\mathbf{y})}{\omega - \omega_m - \mathrm{i}\gamma_m} \frac{u_i^l(\mathbf{x})\, u_j^l(\mathbf{y})}{\omega - \omega_l - \mathrm{i}\gamma_l} \frac{u_i^k(\mathbf{x})\, u_j^k(\mathbf{y})}{\omega - \omega_k - \mathrm{i}\gamma_k}. \tag{11}$$

We again invoke the lack of spatial correlations amongst the eigenfunctions and find that the only terms which survive an average are the $r = m = l = j$ terms, and the $r = m \neq l = k$, the $r = l \neq m = k$, and the $r = k \neq m = l$ terms. Re-labelling some of the indices we find

$$\langle T^2 \rangle = \sum_r \frac{\langle u_i^r(\mathbf{x})^4 \rangle \langle u_j^r(\mathbf{y})^4 \rangle \equiv \langle u^4 \rangle^2}{(\omega - \omega_r - \mathrm{i}\gamma_r)^2 (\omega - \omega_r + \mathrm{i}\gamma_r)^2}$$

$$+ 2 \sum_{r \neq 1} \frac{\langle u^2 \rangle^4}{(\omega - \omega_r - \mathrm{i}\gamma_r)(\omega - \omega_r + \mathrm{i}\gamma_r)(\omega - \omega_l - \mathrm{i}\gamma_l)(\omega - \omega_l + \mathrm{i}\gamma_l)}$$

$$+ \sum_{r \neq 1} \frac{\langle u^2 \rangle^4}{(\omega - \omega_r - \mathrm{i}\gamma_r)^2 (\omega - \omega_l + \mathrm{i}\gamma_l)^2}. \tag{12}$$

The first of these terms is readily averaged over ω_r, as previously, by inserting a factor of D, dropping the summation sign, and integrating over ω_r. The other terms require an integration over both ω_r and ω_l. As emphasized by Davy [1] and by Weaver [6], it is important to take account of eigenfrequency correlations. The average of a sum over two eigenfrequencies in a GOE spectrum is given by two factors of D, one factor of $[1 - Y_2\{D(\omega_r - \omega_l)\}]$ and an integration over all ω_r and ω_l. Y_2 is the Dyson two-level correlation function [8, 9]. It vanishes at $\pm\infty$, is an even function of its argument, and equals unity at zero:

$$\begin{aligned}\langle T^2\rangle = D\langle u^4\rangle^2 \int_{-\infty}^{+\infty} \frac{\mathrm{d}\alpha}{(\alpha - \mathrm{i}\gamma)^2(\alpha + \mathrm{i}\gamma)^2} \\ + 2D^2\langle u^2\rangle^4 \int_{-\infty}^{+\infty}\int_{-\infty}^{+\infty} \frac{[1 - Y_2(Dv)]\,\mathrm{d}v\,\mathrm{d}\alpha}{(\alpha - \mathrm{i}\gamma_r)(\alpha + \mathrm{i}\gamma_r)(\alpha - v - \mathrm{i}\gamma_l)(\alpha - v + \mathrm{i}\gamma_l)} \\ + D^2\langle u^2\rangle^4 \int_{-\infty}^{+\infty}\int_{-\infty}^{+\infty} \frac{[1 - Y_2(Dv)]\,\mathrm{d}v\,\mathrm{d}\alpha}{(\alpha - \mathrm{i}\gamma_r)^2(\alpha - v + \mathrm{i}\gamma_l)^2}.\end{aligned} \tag{13}$$

It is assumed that the modal decay rates γ are uncorrelated with each other and with the proximity of neighboring eigenfrequencies. Thus, the final average over decay rates can be carried out independently of the present average over eigenfrequencies. This assumption is supported by numerical experiments [32].

The integrations over α can be done in closed form:

$$\begin{aligned}\langle T^2\rangle = D\langle u^4\rangle^2 \frac{\pi}{2\gamma_r^3} \\ + 4\pi D^2\langle u^2\rangle^4 \frac{\gamma_r + \gamma_l}{2\gamma_r\gamma_l} \int_{-\infty}^{+\infty} \frac{[1 - Y_2(Dv)]\,\mathrm{d}v}{(v^2 + (\gamma_r + \gamma_l)^2)} \\ + 4\mathrm{i}\pi D^2\langle u^2\rangle^4 \int_{-\infty}^{+\infty} \frac{[1 - Y_2(Dv)]\,\mathrm{d}v}{(v - \mathrm{i}(\gamma_r + \gamma_l)^3)}.\end{aligned} \tag{14}$$

Evaluation of this expression demands the performance of the integration with respect to v, and an average over the values of the γ's.

One simple limit of the above expression is obtained by the approximation $Y_2(\xi) \sim 0$, i.e., in the case that one ignores the eigenfrequency correlations. This has been thought to be valid in the limit of small overlap: $M \ll 1$. In this case, the second of the above integrals over v vanishes and the first may be done easily:

$$\langle T^2\rangle = D\langle u^4\rangle^2 \frac{\pi}{2\gamma_r^3} + \frac{2\pi^2}{\gamma_r\gamma_l} D^2\langle u^2\rangle^4. \tag{15}$$

On averaging over the γ, this becomes

$$\langle T^2\rangle = D\langle u^4\rangle^2 \frac{\pi}{2\bar{\gamma}^3} \frac{n^3}{(n-1)(n-2)(n-3)} + \frac{2\pi^2}{\bar{\gamma}^2} \frac{n^2}{(n-1)^2} D^2\langle u^2\rangle^4. \tag{16}$$

The relative variance is

$$relvar = \frac{\langle T^2\rangle - \langle T\rangle^2}{\langle T\rangle^2} = 1 + \frac{\langle u^4\rangle^2}{\langle u^2\rangle^4} \frac{1}{M} \frac{n(n-1)}{(n-2)(n-3)}, \tag{17}$$

where n is the curvature parameter and M has been defined using the average γ: $M = 2\pi D\bar{\gamma} = \pi D\sigma$.

If we do not neglect Y_2 then the above expression for *relvar* is augmented by terms related to Y_2:

$$relvar = 1 + \frac{\langle u^4\rangle^2}{\langle u^2\rangle^4}\,\frac{1}{M}\,\frac{n(n-1)}{(n-2)(n-3)} - 4/\pi\,\overline{\left[\frac{\gamma_r+\gamma_l}{\gamma_r\gamma_l}\,I_1 + \mathrm{i}I_2\right]}\,\bar{\gamma}^2\,\frac{(n-1)^2}{n^2},$$

where

$$I_1 = \frac{1}{2}\int_{-\infty}^{+\infty}\frac{Y_2(Dv)\,\mathrm{d}v}{(v^2+(\gamma_r+\gamma_l)^2)}, \qquad I_2 = \int_{-\infty}^{+\infty}\frac{Y_2(Dv)\,\mathrm{d}v}{(v-\mathrm{i}(\gamma_r+\gamma_l))^3}, \tag{18}$$

where the overbar indicates an average over the γ. These integrals over v are done most easily by taking advantage of the relatively simple form Y_2 takes when Fourier transformed [9]:

$$b(q) \equiv \tilde{Y}_2(2\pi q) \equiv \int_{-\infty}^{+\infty} Y_2(\xi)\exp\{\mathrm{i}\,2\pi q\xi\}\,\mathrm{d}\xi.$$

$$Y_2(\xi) = \frac{1}{2\pi}\int_{-\infty}^{+\infty}\exp\{-\mathrm{i}\xi q\}\,b(q/2\pi)\,\mathrm{d}q, \tag{19}$$

$$b(q) = \begin{cases} 1 - 2|q| + |q|\ln(1+2|q|) & |q| < 1, \\ -1 + |q|\ln\dfrac{2|q|+1}{2|q|-1}, & |q| > 1. \end{cases}$$

By invoking Parceval's theorem, that the integral of the product of two functions is related to the integral of the product of their Fourier transforms,

$$\int_{-\infty}^{\infty} f(\xi)g(\xi)\,\mathrm{d}\xi = \frac{1}{2\pi}\int_{-\infty}^{\infty}\tilde{f}(q)\tilde{g}^*(q)\,\mathrm{d}q, \tag{20}$$

we find that I_1 and I_2 become

$$I_1 = \frac{1}{4}\int_{-\infty}^{+\infty}\frac{b(q/2\pi)\exp\{-D|q|(\gamma_n+\gamma_l)\}}{(\gamma_n+\gamma_l)}\,\mathrm{d}q,$$

$$I_2 = -\mathrm{i}/2\int_{-\infty}^{0} D^2q^2\,b(q/2\pi)\exp\{-D|q|(\gamma_n+\gamma_l)\}\,\mathrm{d}q. \tag{21}$$

The quantity

$$Q = \overline{\left[\frac{\gamma_r+\gamma_l}{\gamma_r\gamma_l}\,I_1 + \mathrm{i}I_2\right]} \tag{22}$$

then becomes

$$Q = \frac{1}{4}\int_{-\infty}^{\infty} b(q/2\pi)\left[\overline{\frac{\exp\{-D|q|\gamma\}}{\gamma}}\right]^2\mathrm{d}q + \frac{1}{2}\int_{-\infty}^{0} b(q/2\pi)D^2q^2\overline{[\exp\{-D|q|\gamma\}]}^2\,\mathrm{d}q$$

$$= \frac{n^2}{4\bar{\gamma}^2(n-1)^2}\int_{-\infty}^{\infty} b(q/2\pi)(1+D|q|\bar{\gamma}/n)^{2-2n}\,\mathrm{d}q + \frac{1}{2}\int_{-\infty}^{0} b(q/2\pi)D^2q^2(1+D|q|\bar{\gamma}/n)^{-2n}\,\mathrm{d}q$$

$$= \frac{n^2}{2\bar{\gamma}^2(n-1)^2}\int_0^{\infty}\frac{b(q/2\pi)\,\mathrm{d}q}{(1+Dq\bar{\gamma}/n)^{2n-2}} + \frac{1}{2}\int_0^{\infty}\frac{b(q/2\pi)D^2q^2\,\mathrm{d}q}{(1+Dq\bar{\gamma}/n)^{2n}}$$

$$= \frac{2\pi n^2}{2\bar{\gamma}^2(n-1)^2}\int_0^{\infty}\frac{b(t)\,\mathrm{d}t}{(1+Mt/n)^{2n-2}} + \frac{2\pi M^2}{2\bar{\gamma}^2}\int_0^{\infty}\frac{b(t)t^2\,\mathrm{d}t}{(1+Mt/n)^{2n}}. \tag{23}$$

So

$$relvar = 1 + \frac{\langle u^4\rangle^2}{\langle u^2\rangle^4}\;\frac{1}{M}\;\frac{n(n-1)}{(n-2)(n-3)} - \frac{f(M,n)}{M}, \tag{24}$$

where

$$f(M,n) = 4M\left[\int_0^{\infty}\frac{b(t)\,\mathrm{d}t}{(1+Mt/n)^{2n-2}} + M^2\,\frac{(n-1)^2}{n^2}\int_0^{\infty}\frac{b(t)t^2\,\mathrm{d}t}{(1+Mt/n)^{2n}}\right]$$

$$= 4M\left[I_3 + M^2\frac{(n-1)^2}{n^2}I_4\right]. \tag{25}$$

The integrals I_3 and I_4 can be evaluated exactly, for arbitrary M and n, in terms of products of hypergeometric functions and the Beta-function. The results are not simple however, and certain limiting cases are more instructive.

For small M, it may be seen that $f \to 4M\int b(t)\,\mathrm{d}t = 2M$ and *relvar* approaches a simple limiting expression

$$relvar = \frac{n(n-1)}{(n-2)(n-3)}\;\frac{K^2}{M} - 1 + O(M), \quad M \ll 1. \tag{26}$$

At modest levels of decay curvature, for example at $n = 10$, this is about $-1 + 14.5/M$, which may be compared with the conventional prediction case: $1 + 9/M$. It is clear that decay curvature has a significant impact on the theoretical prediction for *relvar*. It is also apparent that the earlier estimate for the low M limit $(1 + 9/M)$ is valid only at order $1/M$, not at order unity.

For large M the integrals I_3 and I_4 are, to leading order, $(n/M)/(2n-3)$ and $(2n/M)^3/(2n-3)(n-1)(2n-1)$ respectively. Thus *relvar* is

$$relvar = 1 + \frac{1}{M}\left[K^2\;\frac{n(n-1)}{(n-2)(n-3)} - \frac{4n(3n-2)}{(2n-3)(2n-1)}\right] + o(1/M), \quad M \gg 1. \tag{27}$$

In agreement with previous results [6], this becomes $1 + (K^2 - 3)/M$ in the limit of no curvature, $n = \infty$.

The case of weak curvature, n large but not infinite, at arbitrary M, is also relevant. In this case we can expand in powers of $p = 1/n$ for arbitrary M:

$$f(M,n) \approx f(M,n)|_{p=0} + p\;\left.\frac{\partial f}{\partial p}\right|_{p=0} \tag{28}$$

$$= 4M\int_0^{\infty} b(t)[1 + M^2t^2]\mathrm{e}^{-2Mt}\,\mathrm{d}t + p4M\int_0^{\infty} b(t)\mathrm{e}^{-2Mt}[2Mt - M^2t^2 + \tfrac{1}{2}M^4t^4]\,\mathrm{d}t.$$

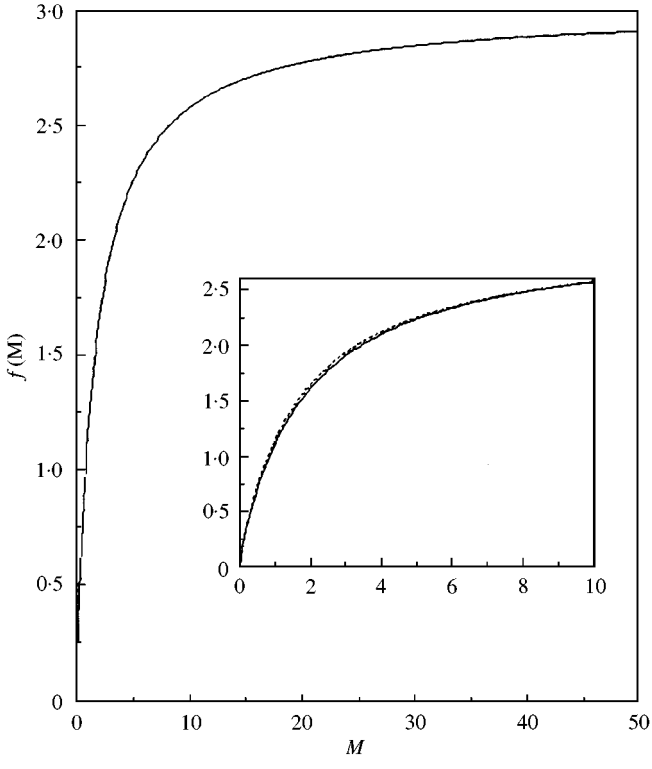

Figure 6. The function $f(M, n = \infty)$. An analytic expression for f is given in equation (30). On the inset $f(M)$ for finite n (- - - -) as calculated using the approximation $b(t) = \exp(-2|t|)$ is also shown; it is barely distinguishable from the exact $f(M, \infty)$. The difference between them, $f_{approximate} - f_{exact}$, peaks at about 0·0419 at $M = 1{\cdot}3$.

Each of these integrations may be evaluated in terms of the usual exponential function E_1 defined by

$$E_1(z) \equiv \int_z^\infty \frac{\exp(-t)}{t}\,\mathrm{d}t, \quad z > 0. \tag{29}$$

The first term is the simpler; at $n = \infty$ and all M, f is given by

$$\begin{aligned} f(M) &= 4M \int_0^\infty b(t)[1 + M^2t^2]\mathrm{e}^{-2Mt}\,\mathrm{d}t \\ &= \left(\frac{M}{4} + 2 - \frac{5}{4M}\right) + \mathrm{e}^{-2M}\left(\frac{M}{4} + \frac{1}{2} + \frac{5}{4M}\right) \\ &\quad - E_1(M)\mathrm{e}^{-M}\left(\frac{M^2}{4} + \frac{3M}{4} + \frac{5}{2} + \frac{5}{2M}\right) - E_1(M)\mathrm{e}^{M}\left(\frac{M^2}{4} + \frac{3M}{4} + \frac{5}{2} + \frac{5}{2M}\right) \end{aligned} \tag{30}$$

which is confirmed by numerical evaluations of the integral. $f(M, n = \infty)$ is plotted in Figure 6. As expected, it smoothly and monotonically varies from 0 to 3.

A useful approximate closed-form expression for $f(M, n)$ for arbitrary M and n is provided by substituting a form for $b(t)$ that makes the integrals (25) tractable. We have found that $b(t) \sim \exp(-2|t|)$ is a pretty good approximation; $\exp(-2|t|)$ correctly describes

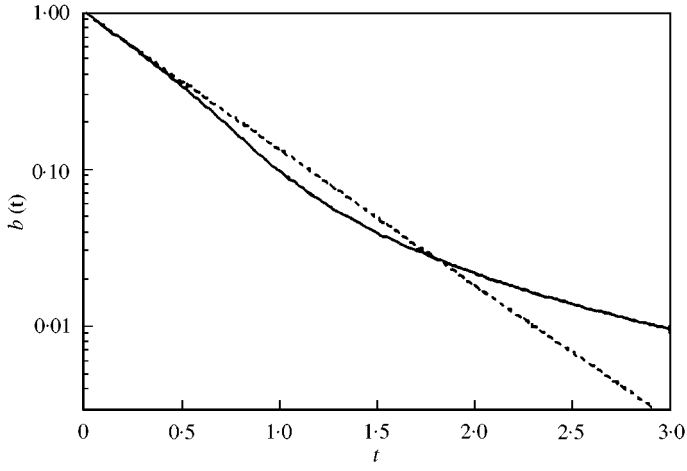

Figure 7. The exact $b(t)$ (solid line, given in equation (19)), is compared with the approximation $\exp(-2|t|)$ (- - - -).

the total integral of $b(t)$, its value at $t = 0$, and also its slope at $t = 0$. Figure 7 provides a more detailed comparison. The inset to Figure 6 compares $f(M, n = \infty)$ as obtained exactly, and as obtained using this approximation for $b(t)$. The difference is small.

After making the substitution $b(t) \sim \exp(-2|t|)$, the integrals I_3 and I_4 may be performed for arbitrary n in terms of the generalized exponential functions $E_j(z) \equiv \int_1^\infty t^{-j} \exp\{-zt\}\, dt$:

$$I_3 = \frac{n}{M} \exp\{2n/M\}\, E_{2n-2}(2n/M),$$

$$I_4 = \frac{n^3}{M^3} \exp\{2n/M\}\, [E_{2n}(2n/M) - 2E_{2n-1}(2n/M) + E_{2n-2}(2n/M)]. \qquad (31)$$

To summarize, the relative power variance for a system with GOE eigenfrequency statistics Y_2, and chi-square width statistics (1), is given exactly by equation (24). The function $f(M, n)$ is defined by equation (25). In the limit of no decay curvature ($n = \infty$), f is given by the simple expression (30). In the limit of small M, but arbitrary decay curvature, the relative variance is given exactly by equation (26). For all M and n, f is given approximately by equation (25) and (31). Figure 8 plots $f(M, n)$ versus M for various relevant values of n, and also plots the approximate expressions (25) and (31). It is seen that the approximate expression is reasonably accurate over the full range examined.

3.2. COMPARISON WITH MEASURED POWER VARIANCES

In Figure 9 we plot the observed relative variance versus frequency, and also plot the theoretical value (24) where $M = \pi D\sigma$ and n and σ are taken from fits of the observed diffuse field decay to formula (2), and D is taken from equation (3). The correspondence is less close than it was in Figure 5. The data support the theory is certain ways, and show the predicted transition between low M and high M behavior, but nevertheless the data lie consistently below theoretical predictions. Consideration of decay curvature has in fact led to less agreement between theory and measurement.

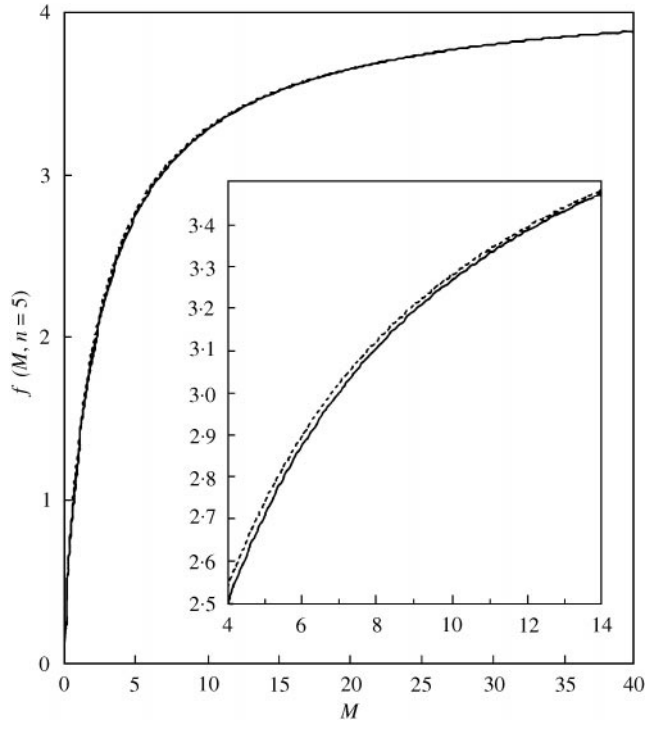

Figure 8. The function $f(M, n)$ is plotted (——) versus M at $n = 5$. Its approximate version (- - - -) based on the substitution $b(t) = \exp(-2|t|)$ is also plotted. The difference is small.

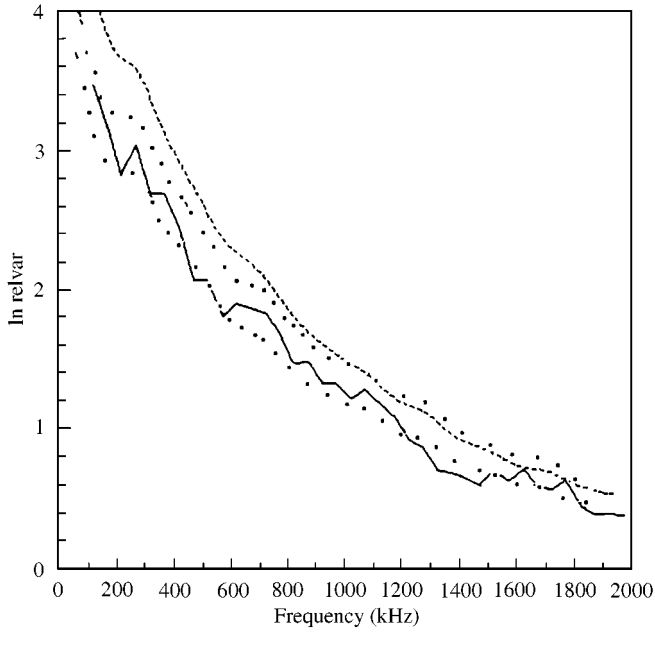

Figure 9. The experimentally determined *relvar* (——) is compared with the new and more precise theory (- - - -) that incorporates decay curvature and a precise analysis of the transition between low and high modal overlap limits. The correspondence with the measurement is now poor. The isolated dots indicate the predictions of the earlier theory (Figure 5).

3.3. DISCUSSION

We have examined several hypotheses in an attempt to understand the lack of accord between theory and measurements. They are (1) temperature variations during the tests, (2) correlations between γ and u, (3) correlations between source and receiver positions $\mathbf{x}$ and $\mathbf{y}$, (4) error in the theory where the integrand was approximated by its form in the vicinity of the dominating reasonances, (5) that our estimates for D are in error, and (6) that the modal amplitude statistics are non-Gaussian; $K \neq 3$.

Temperature variations during a test can lead, by means of the temperature sensitivity of the resonant frequencies, to artificially augmented resonance widths, widths that are unrelated to decay. Thus, the measured relative variances would be less than they ought to be. This is indeed an effect, but it was found to be small. We learned to control it by conducting tests in a container that minimized air drafts and by monitoring the sample temperature.

If γ_m is correlated with $u_m(\mathbf{x})$ or $u_m(\mathbf{y})$, our theory would be in error. Such correlation could follow if the source or detector contributed significant amounts of dissipation, because the modes which the tranducers are most sensitive to have extra dissipation. Our test were normally conducted using "dry-coupled" transducers. However, when we did add a small drop of oil or water to the transducer/sample contact, we found that the signal was much stronger, the decay was faster, and the decay had more curvature. All these effects are consistent with a hypothesis of dissipative processes taking place at the liquid drop. The effect on *relvar* was strong — the measured *relvar* values were even less in agreement with theory than they had been. A drop of oil placed at a point away from source or receiver contributed less to the decay and had essentially no effect on the agreement or lack thereof between theory and measured *relvars*. Thus γ–u correlations can be attributed to the wet-contact transducers. The question remains as to whether the dry-coupled tranducers also have such correlations. We answer that in the negative by a simple test in which a third (also dry-coupled) dummy transducer is placed on the sample. This was found to make no measurable difference in the system σ. Thus, there is no dissipation associated with our dry coupling, and γ–u correlations are not present.

The theory also assumed that the source and receiver are sufficiently distant so that there are no correlations between $u_r(\mathbf{x})$ and $u_r(\mathbf{y})$; i.e., $\langle u_r(\mathbf{x})\, u_r(\mathbf{y})\rangle = 0$. In actually, source and receiver were typically separated by distances of the order of 15 mm. It is well established that such correlations do exist, but that they decay on a length scale of the order of a wavelength. Numerical simulations in 2-D corroborate the usual prediction that the u's are Gaussian and have correlations given by

$$\langle u_r(\mathbf{x})\, u_r(\mathbf{y})\rangle = \langle u^2\rangle (1 + J_0(k|\mathbf{x} - \mathbf{y})|)). \tag{32}$$

If we apply this to our system and take the modes to have their correlations on the surface dominated by those of the Rayleigh surface waves, we find that the predictions for *relvar* should be greater by about 10% for source and receiver at a distance of two Rayleigh wavelengths. (This is surely an overestimate, as only part of the surface disturbance is Rayleigh waves). We conclude that the effect is weak, especially for frequencies above 400 kHz, but that in any case it has the wrong sign; it lead to worse agreement between theory and measurement.

The power transmission function $T(\omega)$ is clearly dominated by the contribution of the modes m that have frequencies ω_m close to ω. Nevertheless, the distant modes do contribute [31], and the theory presented above has approximated their contribution. We have re-examined the theory without making the approximation and found that the error

incurred by the approximation is indeed small compared to the large discrepancy we have between theory and measurement.

The value of D used in constructing M was based on an asymptotic Weyl formula that is not exact. Any error there must, however, be quite small. The Weyl formula has been checked in detail over the regime from 100 to 200 kHz where individual peaks were distinct enough to allow it, and errors were found to be far smaller than the discrepancies we seek to explain.

It may be noted that the theory for *relvar* entails a ratio of the ensemble average of the square of T to the square of its ensemble average. The quantities plotted here are, however, spatial averages of the ratio of short-frequency-range averages. These are not precisely equivalent. The spatial average is not a problem, as it only smooths out fluctuations in *relvar*. The frequency average is, as argued here and elsewhere, equivalent to an ensemble average. The average of a ratio is not, though, the same as the ratio of the averages. A closer scrutiny of the approximation reveals that it artificially decreases the effective value of K^2. Indeed, if there were only one peak in the range $\{f_1 \rightarrow f_2\}$ the effective K^2 would be 1. The effective K^2 may be calculated by a simple Monte-Carlo construction of the ratio of the average of the fourth powers of a finite number N of random numbers r, to the square of the average of the squares of those numbers r, where each random number r is itself the product of two Gaussian random numbers. The effective K^2 rapidly approaches 9 as the number of peaks N in the range $\{f_1 \rightarrow f_2\}$ increases. At 100 kHz, the number of peaks in the range is about $N = 45$, where the effective K^2 is about 6·5. At 200 kHz, there are about $N = 128$ peaks in the range, and $(K^2)_{effective}$ is 7·9. At 300 and 400 kHz these quantities are 248 (8·3) and 406 (8·5) respectively. Thus, the difference between the ratio of the averages and the average of the ratios is not enough to explain the discrepancy between the theory and measurements.

We are left with one hypothesis: that the mode shapes are not Gaussian; that, as Davy suggested phenomenologically in order to make his theory conform to his measurements [2], $K^2 < 9$. Militating against this hypothesis is the excellent agreement between the spectral correlations of block A and those of the GOE [7]. It would be peculiar if the GOE predictions for spectral correlations were so well followed, while the modal amplitude statistics are not. Also militating against the hypothesis is the central limit theorem and a vague notion that Gaussian statistics are virtually ubiquitous. These arguments are of course not compelling. In support of the hypothesis we offer three pieces of evidence.

In the regime between 100 and 200 kHz where the peaks are well separated, and width and amplitude values can be measured directly from the spectra, we found that the average and standard deviation of the peak widths agreed with the γ statistics assumed in equation (2). The same data were also used to extract values for, and statistics on, $|u_n(\mathbf{x})\, u_n(\mathbf{y})|^2$. We found $\langle |u_n(\mathbf{x})\, u_n(\mathbf{y})|^4 \rangle / \langle |u_n(\mathbf{x})\, u_n(\mathbf{y})|^2 \rangle^2 \approx 7$. This is less than 9, but not sufficient to explain the discrepancies we wish to explain. The value ≈ 7 is, though, in agreement with the predicted value of $(K^2)_{effective}$ discussed above. Difficulties recur, then, after one realizes that the distance between $\mathbf{x}$ and $\mathbf{y}$ is comparable to a wavelength at these frequencies and K^2 should be larger than 9 here.

When the source and receiver are placed on the corners of the sample the signal is much greater. This is not unexpected: modal amplitudes are higher near traction-free surfaces. The measured values of *relvar* are, however, less than they are when the source and receiver are in the interior. The decay and frequency correlation statistics are of course the same in the corners, only the amplitude statistics can differ.

If the modal amplitude statistics are not in accord with random matrix theory (RMT), then it may be that diffuse scattering mechanisms in the sample are not sufficiently strong. The conventional understanding, the "Bohigas Conjecture" [14, 15], asserts that a system with chaotic ray trajectories will be in accordance with RMT, except on the longest frequency scales — those comparable to the inverse of the period of the shorter periodic

orbits. This has been widely confirmed in numerical studies of two-dimensional scalar systems [20–22]. Laboratory confirmations are mostly confined to confirmation of predictions of eigenfrequency correlations [7, 12, 13]. Nevertheless, there are some laboratory studies of the Gaussian nature of the amplitude statistics [11]. We can treat this as well established.

Block A, used in the above study, does not have conventional chaotic ray trajectories. Bohigas *et al*. remarked that the system is not of the usual class [16]. Nevertheless, there is reason to think it ought to have sufficient diffuse scattering mechanisms. Its level statistics suggest that this is the case. Furthermore, the edges of the slit and the corners of the block do generate diffuse scattering. As discussed in references [17, 18] even a point scatterer is somewhat effective. As discussed by many, pseudo-integrable systems without chaotic ray trajectories often have good GOE level statistics. The extend to which Block A is integrable would in any case tend to increase the theoretical prediction for *relvar*.

Even if such systems do have good GOE level statistics, it is not clear that this implies that they ought to have GOE amplitude statistics. To explore this possibility we have also measured *relvar* for some other elastic bodies. Block "B" from the previous study has two slits cut into it and presumably has more diffuse scattering. Block "X" with several slits was also constructed, and also Block "D" with defocusing surfaces, both with sizes comparable to those of B and A (23 cm^3). A large block ("E") was also constructed, with diffusing surfaces, and volume $\sim 2200\ cm^3$. The decay curvature for this specimen was much less, with values of $n > 30$ over all frequencies investigate. For all these specimens we found that the theory and measurement for *relvar* remained in poor accord. The conclusion is that the above theory is still inaccurate. The poor accordance with theory remains unexplained.

4. CONCLUSIONS

The theory presented here is arguably much more realistic than that employed by Lyon [4] and Davy [1–3]; we have included the proper GOE eigenfrequency correlations; we have replaced the assumption $K = 27/8$ with a more reasonable value $K = 3$; we have incorporated modal width variations. Nevertheless, just as observed by Davy in acoustic reverberation rooms [1], the predicted variances exceed the measured variances. It is outside the scope of this paper to pursue this matter further, but we do conclude with a speculation.

The theory presented here, as well as that of Lyon and Davy, assumed that the modes were real, uncoupled by the dissipation. It is extraordinarily unlikely that the dissipation is simultaneously diagonalizable with the rest of the dynamics. In other words, the actual modes must be complex. The appropriate definition of K would then be $\langle |u(\mathbf{x})|^4 \rangle / \langle |u(\mathbf{x})|^2 \rangle^2$. If the real and imaginary parts of u are independent Gaussian random numbers, this quantity lies between 2 and 3, depending on the relative strengths of the real and imaginary parts. At high modal overlap one would imagine that the real and imaginary parts would be of equal strength, and K would be 2. At low modal overlap where the modes are presumably mostly real, K would be closer to 3. The effect moves theory closer to measurement; it remains for more detailed calculations to explore the speculation further.

ACKNOWLEDGMENT

The authors thank Oliver Legrand for helpful discussions. This work was supported by the grant number 9701142 from the National Science Foundation.

REFERENCES

1. J. L. DAVY 1986 *Journal of Sound and Vibration* **107**, 361–373. The ensemble variance of random noise in a reverberation room.
2. J. L. DAVY 1987 *Journal of Sound and Vibration* **115**, 145–161. Improvements on formulae for the ensemble relative variance of random noise in a reverberation room.
3. J. L. DAVY 1981 *Journal of Sound and Vibration* **77**, 455–479. The relative variance of the transmission function of a reverberation room.
4. R. H. LYON 1969 *Journal of the Acoustical Society of America* **45**, 545–565. Statistical analysis of power injection and response ion structures and rooms.
5. R. V. WATERHOUSE 1978 *Journal of the Acoustical Society of America* **64**, 1443–1446. Estimation of monopole power radiated in a reverberation chamber.
6. R. L. WEAVER 1989 *Journal of Sound and Vibration* **130**, 487–491. On the ensemble variance of reverberation room transfer functions, the effect of spectral rigidity.
7. R. L. WEAVER 1989 *Journal of the Acoustical Society of America* **85**, 1005–1013. Spectral statistics in elastodynamics.
8. M. L. MEHTA 1990 *Random Matrices*. Boston: Academic Press.
9. T. A. BRODY, J. FLORES, J. B. FRENCH, P. A. MELLO, A. PANDEY and S. S. M. WONG 1981 *Reviews of Modern Physics* **53**, 385–478. Random matrix physics: spectrum and strength fluctuations.
10. J. L. DAVY 1990 *Proceedings of the International Conference on Noise Control Engineering. Inter-noise* 1990, Vol. 1, Poughkeepsie, NY, 159–164. The distribution of modal frequencies in a reverberation room.
11. A. KUDROLLI, V. KIDAMBI and S. SRIDHAR 1995 *Physical Review Letters* **75**, 822–825. Experimental studies of chaos and localization in quantum wave functions.
12. C. ELLEGAARD, T. GUHR, K. LINDEMANN, H. Q. LORENSEN, J. NYGÅRD and M. OXBORROW 1995 *Physical Review Letters* **75**, 1546–1549. Spectral statistics of acoustic resonances in aluminum blocks.
13. C. ELLEGAARD, T. GUHR, K. LINDEMANN, J. NYGÅRD and M. OXBORROW 1996 *Physical Review Letters* **77**, 4918–4921. Symmetry breaking and spectral statistics of acoustic resonances in quartz blocks.
14. G. CASATI, F. VALZ-GRIS and I. GUARNIERI 1980 *Lettre al Nuova Cimenti* **28**, 279–282. On the connection between quantization of nonintegrable systems and statistical theory of spectra.
15. O. BOHIGAS, M. J. GIANNONI and C. SCHMIT 1984 *Physical Review Letters* **52**, 1–4. Characterization of chaotic quantum spectra and universality of level fluctuation laws.
16. O. BOHIGAS, O. LEGRAND, C. SCHMIT and D. SORNETTE 1991 *Journal of the Acoustical Society of America* **89**, 1456–1458. Comment on spectral statistics in elastodynamics.
17. R. L. WEAVER and D. SORNETTE 1995 *Physical Review E* **52**, 3341–3350. The range of spectral correlations in pseudointegrable systems: GOE statistics in a rectangular membrane with a point scatterer.
18. O. LEGRAND, F. MORTESSAGNE and R. L. WEAVER 1997 *Physical Review E* **55**, 7741–7744. Semiclassical analysis of spectral correlations in regular billiards with point scatterers.
19. T. CHEON and T. D. COHEN 1989 *Physical Review Letters* **62**, 2769–2772. Quantum level statistics of pseudointegrable billiards.
20. E. J. HELLER 1986 in Quantum *Chaos and Statistical Nuclear Physics* (T. H. Seligman and H. Nishioka, editors), Lecture Notes in Physics, Vol. 263, 162–181. New York: Springer. Qualitative properties of eigenfunctions of classically chaotic Hamiltonian systems.
21. S. W. MCDONALD and A. N. KAUFMANN 1979 *Physical Review Letters* **42**, 1189–1192. Spectra and eigenfunctions for a Hamiltonian with stochastic trajectories 1988 *Physical Review A* **37**, 3067–3083.
22. R. L. WEAVER 1993 *Structural Dynamics of Large Scale and Complex Systems*, (C. Pierre and N. Perkins, editors), 35–42. *Proceedings of the* 14*th Biennial Conference on Vibrations and Noise, Albuquerque September* New York: ASME. On eigenmode statistics and power variances in randomly shaped membranes.
23. O. BOHIGAS 1991 in *Chaos & Quantum Physics*, 1–117. Les Houchjes Session LII: Elsevier, Random matrix theories and chaotic dynamics.
24. R. WEAVER 1996 in *Localization and the Effects of Irregularities in structures. Applied Mechanics Review* **99**, 111–120. Localization, scaling, and diffuse transport of wave energy in disordered media.

25. R. H. LYON and R. G. DEJONG 1995 *Theory and Application of Statistical Energy Analysis*. Boston MA: Butterworths-Heimann.
26. R. WEAVER 1986 *Journal of the Acoustical Society of America* **79**, 919–923. Laboratory studies of diffuse waves in plates.
27. J. BURKHARDT and R. L. WEAVER 1996 *Journal of Sound and Vibration* **196**, 147–164. The effect of decay rate variability on statistical response predictions in acoustic systems.
28. J. BURKHARDT 1986 *Ultrasonics* **36**, 471–475. Damage assessment using reverberant decays.
29. R. WEAVER 1982 *Journal of the Acoustical Society of America* **71**, 1608–1609. On diffuse waves in solid media.
30. M. DUPUIS, R. MAZO and L. ONSAGER 1960 *Journal of Chemical Physics* **33**, 1452–1462. Surface specific heat of an isotropic solid at low temperature.
31. J. L. DAVY 1999 *Private communication.*
32. J. BURKHARDT and R. WEAVER 1996 *Journal of the Acoustical Society of America* **100**, 320–326. Spectral statistics in damped systems, Part I. Model decay rate statistics.